Electronic Supplementary Material (ESI) for Green Chemistry.

Electronic Supplementary Information (ESI)

Solution Processing V_2VI_3 Chalcogenides with Deep Eutectic Solvent for Enhanced Visible-Light-Driven Hydrogen Production

Jinfang Wang[a] and Hongyu Mou[a, b] Rong Li,[c] Yan Li,[d] Debao Wang,[b] Zhimin Xue,[c] Tiancheng Mu*[a]

*Corresponding author. Tel: 86-10-62514925, Email: tcmu@ruc.edu.cn;

Table of the contents

1. Experiment Section

Chemicals and Materials.

The V_2VI_3 compounds were purchased from Sigma Aldrich (St. Louis, USA). Bi_2E_3 (E = S, Se, Te) was finely ground in an agate mortar and pestle for 0.5-1 h. Other V_2VI_3 compounds were used as supplied. 1, 8-diazabicyclo-[5.4.0] undec-7-ene (DBU, 98%) and N-Methylthiourea (97%) were purchased from J&K Scientific Ltd. The DBU was dried in a vacuum at 40 °C for about 12 h and placed in desiccators. Above reagents were stored in desiccators.

Solvent Preparation and V_2VI_3 Compounds Dissolution.

The DES was prepared by the simple mixing of DBU with N-Methylthiourea at 30 °C for about 0.5 h. The solvent was bubbled with N_2 for 24 h at room temperature to remove trace amount of water before use. Then 50 mg V_2VI_3 compounds were added to the solvent (1 g) with agitation at 95 °C for different time (see table S1). For As_2S_3 and Sb_2Se_3, more quantity of solute need to add in the solution until it is saturation. For other chalcogenides, there remained undissolved solid, so the saturated solution was filtered prior to use. The concentration of V_2VI_3 compounds was determined by preparing saturated dispersion and running thermogravimetric analysis (TGA Q500) on the liquid. The residual mass (Figure S5) at 450 °C was taken as representative of the concentration of the chalcogenide.[1] Each reported datum was the average value of three independent measurements with deviation less than 0.1%.

Recovery of Chalcogenide Solid from Solution

To prepare solid for XRD analysis, V_2VI_3 solution (0.5 -1 mL) was placed in a quartz boat under flowing nitrogen, slowly heated to 300-370 °C (ca. 2 h, 300 °C for As_2Se_3, 320 °C for As_2S_3, 340 °C for As_2Te_3, and 370 °C for all others) at which point heating was terminated with a tube furnace (Tianjin Zhonghuan

Lab Furnace Co., Ltd, China). In all cases, the product was powdered before analysis.

Thermal Recovery of Semiconductor Films

Solvent removal entailed heating the drop-cast inks on a temperature-controlled hot plate to 100 °C under flowing nitrogen (3 h). The deposited inks were then annealed on a temperature-controlled hot plate slowly to 350-375 °C under flowing nitrogen followed by a slow cool down to room temperature.

Instrumentation and characterization

Powder X-ray radiation (pXRD) (Rigaku D/max-2500) patterns for measuring V_2VI_3 films were obtained by using Cu Kα as X-ray radiation under 40 kV and 200 mA. The scanning range is 2θ = 10 - 80° with a step of 2θ = 0.02° and 0.5 s per step. The surface morphology and elemental composition of the samples were analyzed by using a field emission scanning electron microscope (FESEM) (Hitachi SU8010, Hitachi High-technologies Corporation, Japan) at an accelerating voltage of 10 keV. Thermal gravimetric analysis (TGA) was performed by using a thermogravimetric apparatus (Q500, TA Instruments) with heating rate of 10 ^{o}C min^{-1} to 450 °C. The attenuated total reflection infrared spectra (ATR-IR) characterization was carried out using a Fourier transform infrared spectrometer (Nicolet 6700, thermo, USA) with single-crystal ZnSe substrate and an accumulation rate of 40 scans at a resolution of 4 cm^{-1} at room temperature in the spectral range of 650 to 4000 cm^{-1}. Solution ^{1}H NMR experiments were performed on a Bruker DMX 300 NMR spectrometer (300 MHz) with d^6-dimethyl sulfoxide as the standard. Differential scanning calorimetry (DSC) was performed using a Q2000 DSC (TA Instruments-Waters LLC, USA) system at a heating rate of 20 °C min^{-1}. The prepared solvents were cooled to −120 °C before heating up to 60-120 °C. UV-vis Diffuse Reflectance Spectroscopy (DRS) were obtained with a

Varian Cary 5E UV-vis spectrophotometer employing the integration sphere diffuse reflectance attachment (Harrick Praying Mantis Attachment, DRA-2). The finely ground powder samples (~20 mg) were loaded into an in situ cell (Harrick, HVC-DR2) and measured in the 300-1000 nm region with a $BaSO_4$ reflectance standard used as the baseline. Fluorescence (PL) spectra and time-resolved diffuse reflectance (TDR) spectroscopy were recorded on an Edinburgh Instruments FLS980 spectrometer.

Computational methods

All the geometry optimizations have been carried out by employing Gaussian09[2] package. Density functional theory (DFT) has been adopted for the optimizations, where B3LYP method has been used combined with the 6-311++G(d,p)[3] basis set and the pseudopotential (LANL2DZ)[4] basis set. Vibrational frequency calculations have confirmed that the optimized structures were located and characterized as true minima. Electrostatic potential (ESP)[5,6] and atoms in molecules (AIM)[7,8] methods have been investigated by Multiwfn 3.3.9[9] based on wavefunctions generated in the optimization processes.

Measurement of solvatochromic parameters of the solvent system

The solvatochromic parameters of the DBU/MTU were determined by the absorption peaks of two dyes, Nile red (NR) and 4-nitroaniline (NA). The stock solutions were prepared by adding the dyes in methanol, and then 100 μl of the solutions were heated at 30 °C under vacuum for 10 min until dyes left. Then we measured the λ_{max} through a UV-Vis spectrophotometer (Shimadzu UV3600). And the solvatochromic parameters were calculated through the following equations: [10-14]

$$v_{max,\ dye} = 10^4/\lambda_{max,dye} \qquad (1)$$

$$\pi^* = (19.839 - v_{max,NR})/2.991 \qquad (2)$$

$$\alpha = \left(19.9657 - 1.0241\pi^* - v_{max,NR}\right)/1.6078 \qquad (3)$$

$$\beta = 11.134 - \frac{3580}{\lambda_{max,NH_2}} - 1.125\pi^* \qquad (4)$$

Cytotoxicity Test

The cytotoxicity assay was evaluated by 3 - (4,5) - dimethy l-thiazolyl - 2,5-diphenyl-tetra-zolium bromide (MTT) assay (GIBCO, Cat No. V13154) and bovine serum (Kang Yuan Biology, Cat No. 11965118) was selected as the normal cells. Typically, the cells were seeded in 96-well plates and incubated 24 h for cell attachment at 37 ^{o}C with 5% CO_2. Subsequently, DBU/MTU solvent mixture was added to the wells and incubated for another 24 h. To perform , the culture medium with the free solvent was removed and replaced with the new culture medium containing reagents (10 μL) followed by incubation for 4 h at 37 ^{o}C to allow formation of formazan dye. Finally, the optical absorption of formazan at 450 nm was measured by an ELISA reader (Perlong, DNM-9602G).

Photocatalytic hydrogen evolution

The photocatalytic strategy employs recovered Sb_2S_3 nanoparticles as photocatalyst, water as the solvent, and visible light as the driving force, while the use of any costly organic solvents, reducing agents and strong acids as well as the input of thermal/electric energy are no longer required. Generally, 10mg of Sb_2S_3 catalysts were suspended in 10 mL aqueous solution containing 10% of triethanolamine (TEOA) as the sacrificial agent and 10^{-3} M Eosin Y (EY) as sensitizer. The suspension was sealed in a glass vessel and purged with nitrogen for 30 minutes to remove oxygen. After degassing, the vessel was exposed under a 300Wxenon lamp (MAX-302, Asahi Spectra Company, Led.) coupled with a visible light (420-760 nm) to evaluate the photocatalytic activity. The H_2 product was analyzed periodically by gas chromatograph (GC, Agilent 7890A) with a thermal conductivity detector

(TCD).

The apparent quantum efficiency (AQE) was measured under the same photocatalytic reaction conditions. Photon flux of the incident light was determined using an optical power meter (Model: CEL-NP2000, Beijing China Education Au-Light Co., Ltd). In the AQE test, the reaction mixtures were irradiated for 60 min. AQE was calculated using the following equation:

$$AQE = \frac{2 \times the\ number\ of\ evolved\ hydrogen\ molecules}{the\ number\ of\ incident\ photons} \times 100\% \tag{5}$$

Electrochemical analysis

The Mott-Schottky (MS) plots were measured in a 0.5 M Na_2SO_4 (pH = 7) at a frequency of 1000 Hz and amplitude of 10 mV under the dark condition. The carrier density and flat band potentials can be deduced by the Mott-Schottky equation,[15]

$$\frac{1}{C_{sc}^2} = \frac{2}{A^2 q \varepsilon \varepsilon_0 N_d}(E - E_{fb} - \frac{kT}{q}) \tag{6}$$

In which C_{sc} is the space-charge capacitance; ε is the dielectric constant, for Sb_2S_3 is 6.67;[16] ε_0 is the vacuum dielectric constant; *q* is the unit charge, here Take 1.6×10^{-19} C; N_d is the carrier density; E is the applied voltage; E_{fb} is the flat band potential; *k* is the Boltzmann constant; T is the absolute temperature. The flat band potentials can be estimated from the extrapolation of $1/C^2 = 0$ in the plot of $(1/C^2)$ versus V, $E_{fb} = E - kT/q$, and are determined to be −0.13 V and 0.22 V for pristine and recovered Sb_2S_3, respectively. The slope determined from the MS plot is used to estimate the carrier density using the equation,

$$N_d = \frac{2}{q\varepsilon\varepsilon_0}[d\left(\frac{1}{C^2}\right)\Big/dV]^{-1} \tag{7}$$

And it is calculated as 1.12×10^{18} cm^{-3} for recovered Sb_2S_3.

2. Supplementary Figures

In the ATR-FTIR spectra (Figure S1), the slight shifts of stretching vibration peak ν(NH) of MTU in 3400 cm^{-1} and vibration absorption peak ν(CN) of DBU in 1673 cm^{-1} prove the existence of weak interaction between DBU and MTU. Thermogravimetric analysis (TGA) curve (Figure S2) shows that the weight loss peak before and after the mixing is obviously shifted, but the number of peaks does not change. It means that weak interaction existed between the hydrogen donor and acceptor.[17] The slight chemical shift of ^{1}H NMR spectroscopy (Figure S3) at 2.2 ppm on the C6-H of DBU and the disappeared peak at 7.45 ppm on the CH_3N-H of MTU indicate the formation of hydrogen bonding between DBU/MTU.[18] For differential scanning calorimetry (DSC) curve (Figure S4), melt point at -40 °C could be observed. These results confirmed the formation of DES by DBU and MTU.

To realize its ‘green property’ for scalable application, the cytotoxicity of the solvent was testified by a normal cell line of bovine serum cells through 3-(4,5)-dimethyl-thiazolyl-2,5-diphenyl-tetra-zolium bromide (MTT) assay.[19] The results shows DBU caused a decrease in cell viability to 59.5% after incubating cells for 48 hours. And cells viability was almost not affected after adding MTU (cell viability: 55.1%) with the same incubating time. It is much higher than hydrazine (22±1%)[20] as solvent previously reported. This remarkable advantage over traditional solvents for dissolving the chalcogenide semiconductors affords great promise for industrial application.

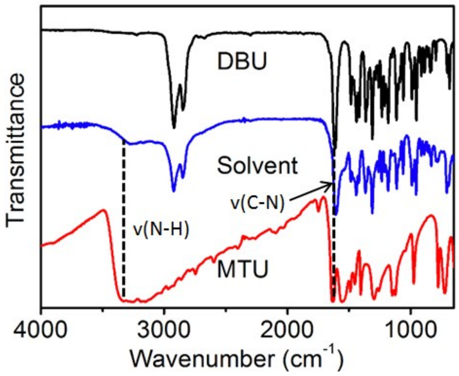

Figure S1. ATR-IR spectra of MTU, DBU and the mixture.[21]

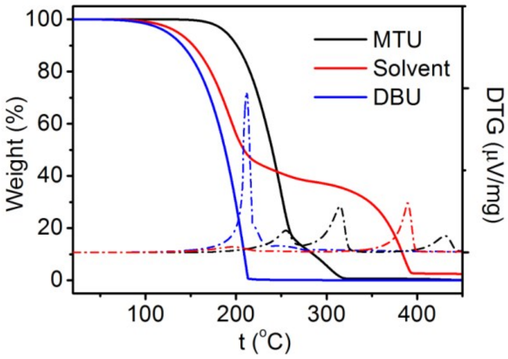

Figure S2. TGA trace of MTU, DBU and the mixture.

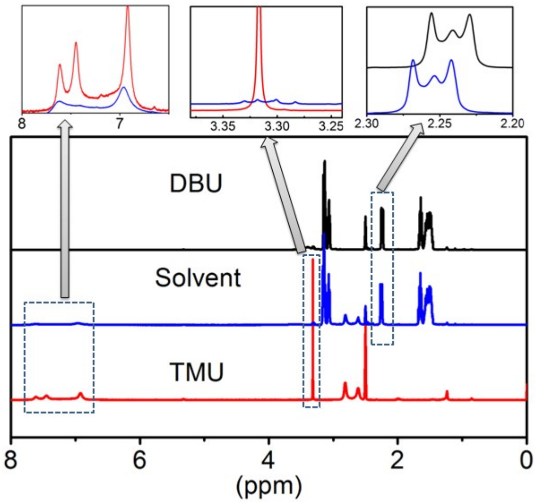

Figure S3. NMR spectra of MTU, DBU and the mixture.

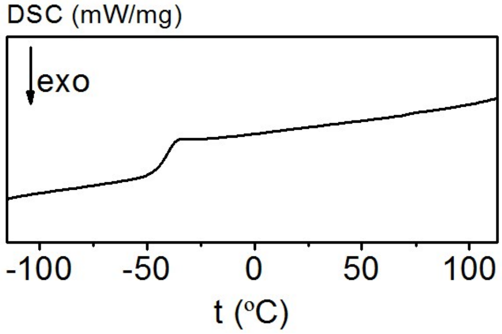

Figure S4. DSC curve of the mixture.

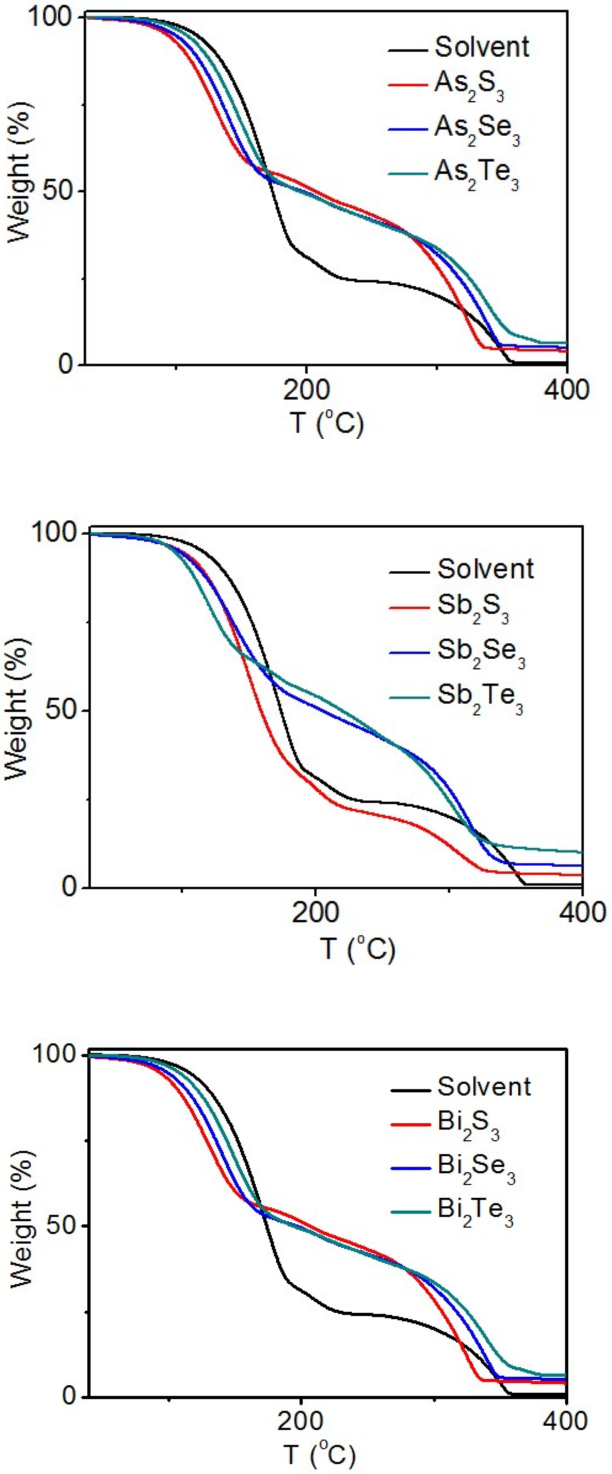

Figure S5. TGA traces of the solid precursors obtained by heat treating saturated solutions of nine V_2VI_3 solutions under nitrogen atmosphere protection.

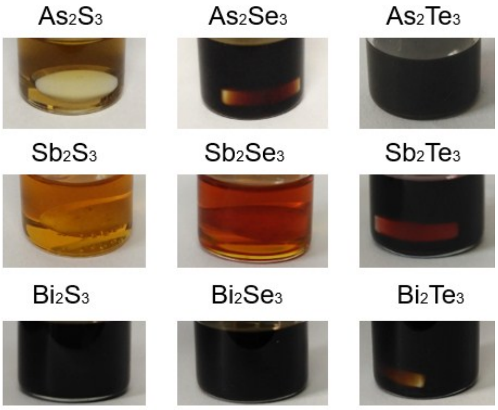

Figure S6. Photograph of saturated solutions of all nine V_2VI_3 semiconductors in DBU/MTU mixture.

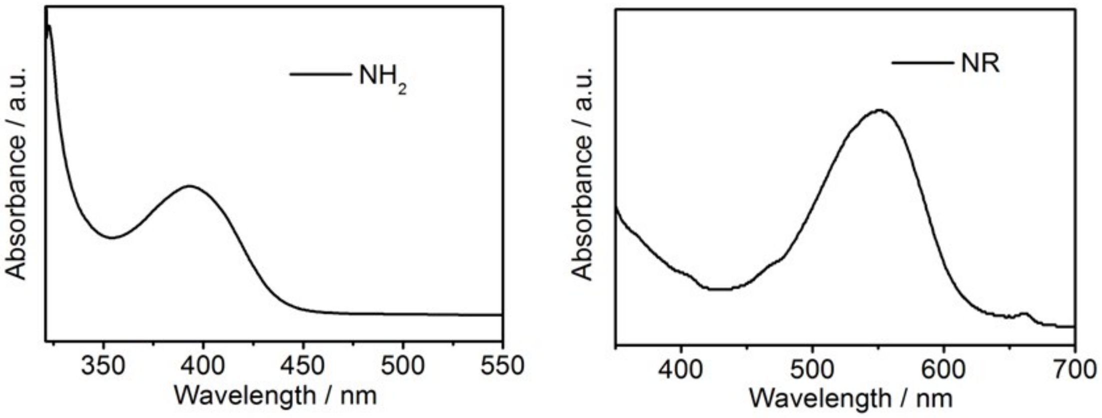

Figure S7. UV-Vis spectra of the mixture after adding Nile red (NR) and *p*-nitroaniline (NH_2).

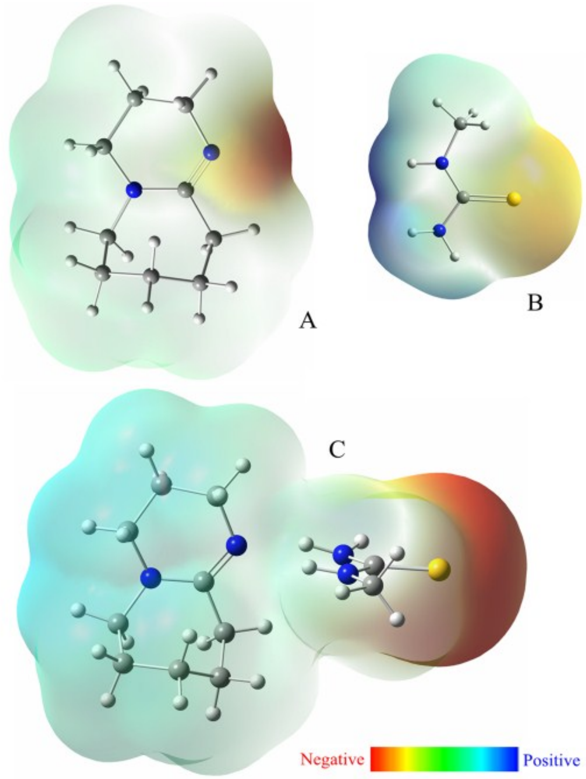

Figure S8. Electrostatic potential distributions on the molecular *van der* Waals (vdW) surface (0.001 isosurface of electron density). A: DBU, B: MTU, C: DBU/MTU mixture.

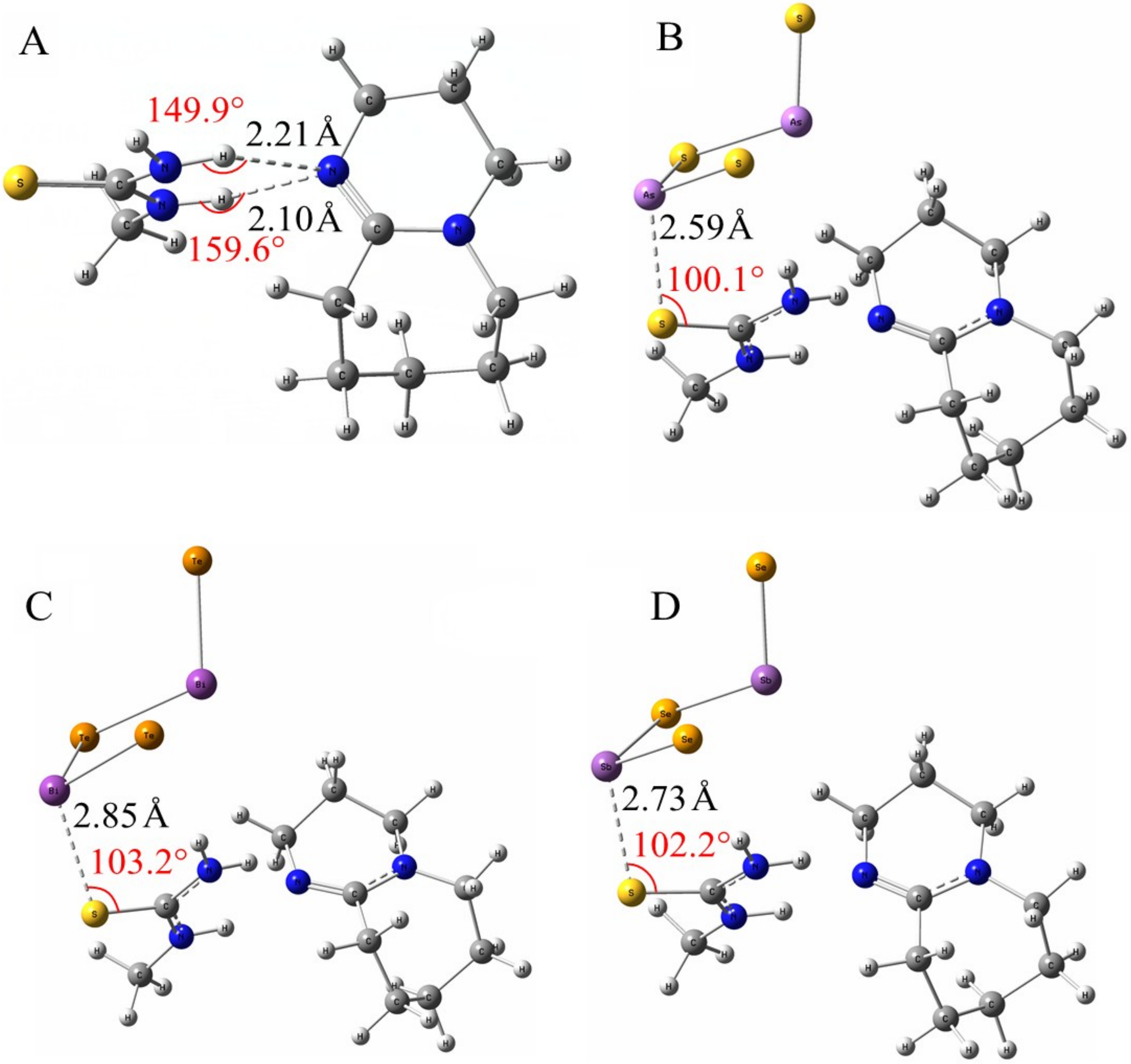

Figure S9. Optimized structures of DES and the complexes formed by DES and three V_2VI_3 chalcogenides. A: DBU/MTU solvent, B: solvent-As_2S_3, C: solvent-Bi_2Te_3, D: splvent-Sb_2Se_3.

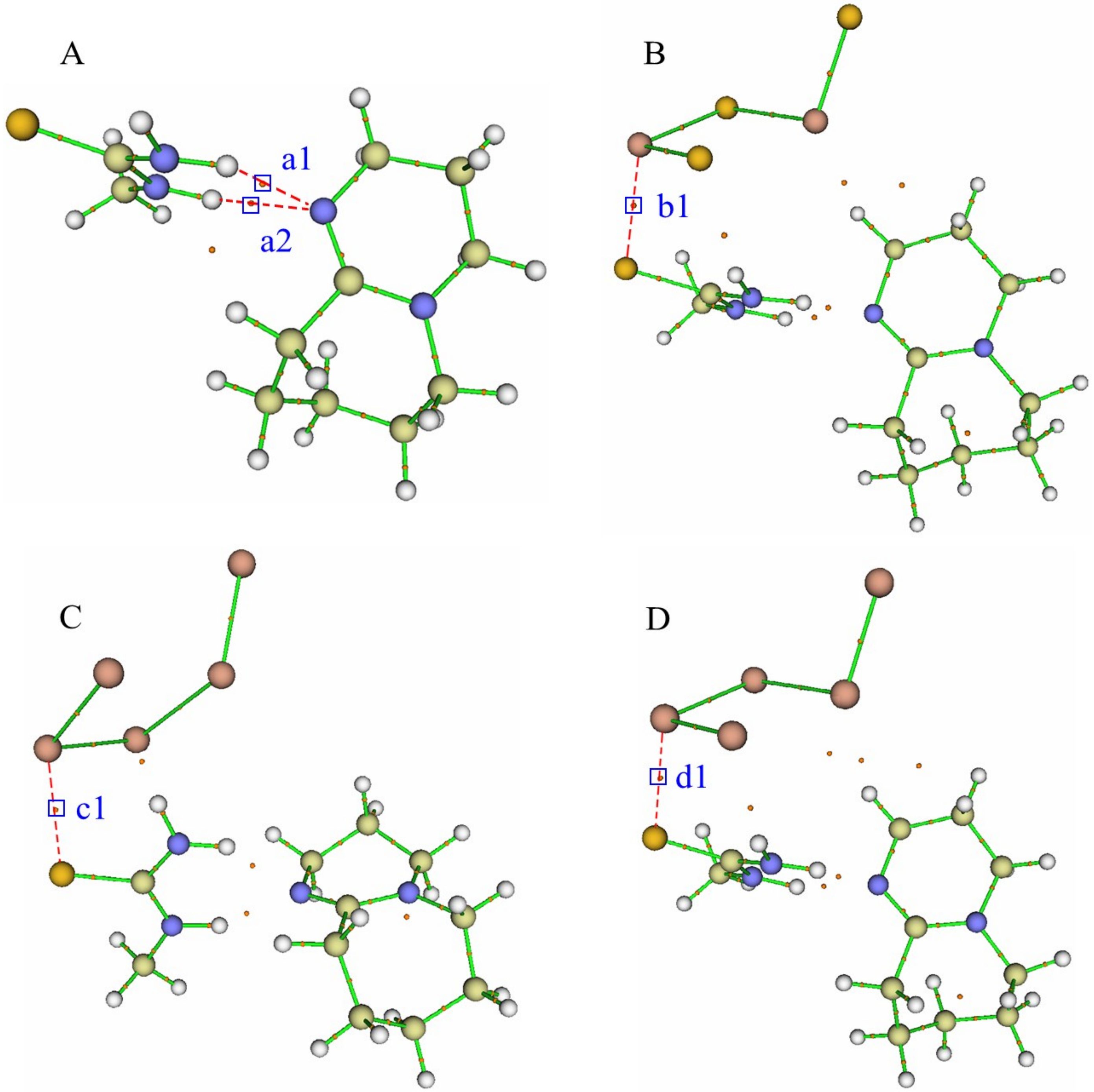

Figure S10. Molecular graphs of DES and the complexes formed by DES and three V_2VI_3 chalcogenides. A: DES, B: solvent-As_2S_3, C: solvent-Bi_2Te_3, D: splvent-Sb_2Se_3. Orange points denote bond critical points.

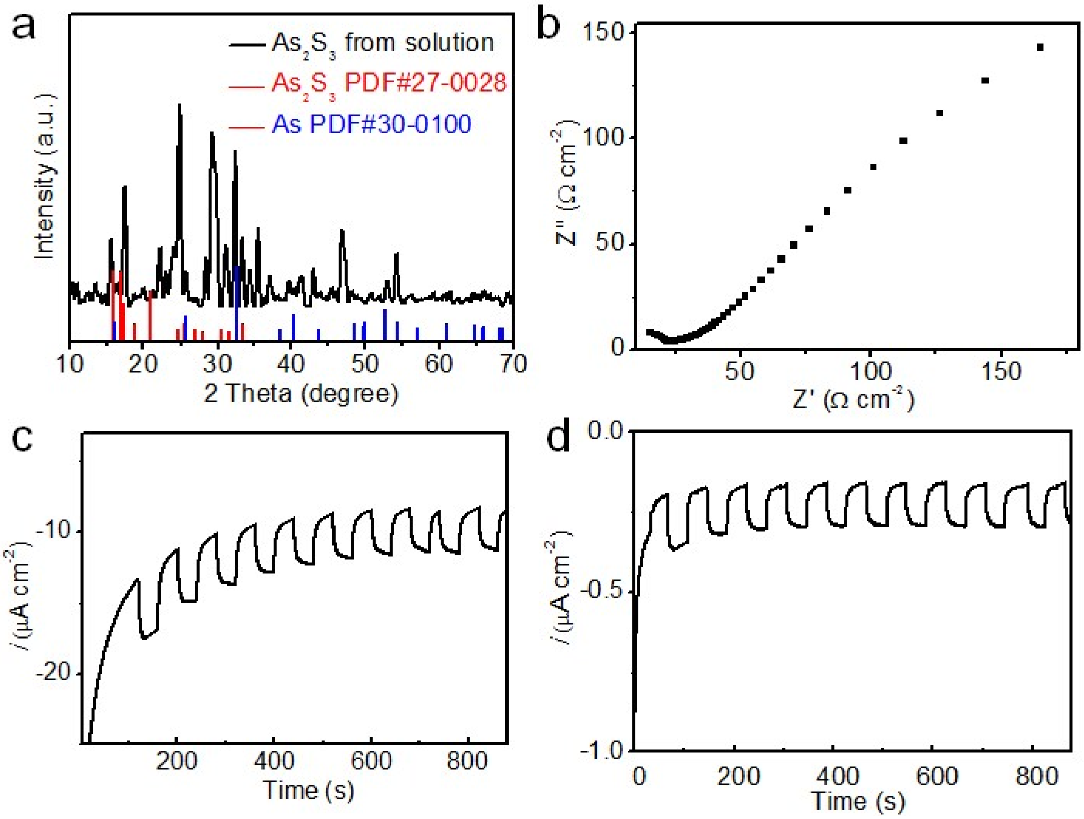

Figure S11. (a) Powder XRD patterns of As_2S_3 deposited from solution and subsequently annealed to 350 °C and stick patterns correspond to orthorhombic As_2S_3 (PDF no. 27-0028) and As (PDF no. 30-0100); (b) Nyquist plot of As_2S_3 film; Transient photoresponse of recovered (c) and pristine (d) As_2S_3 with chopped 1-Sun simulated illumination in contact with 0.1 M $Eu(NO_3)_3$ (aq).

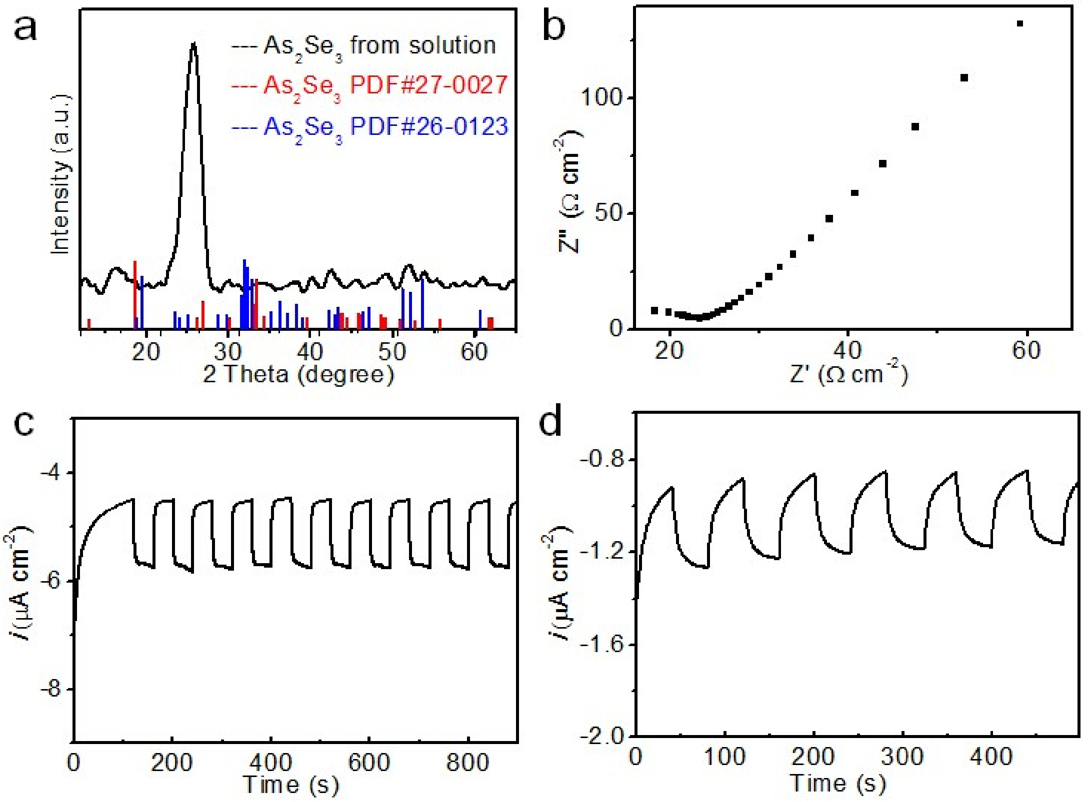

Figure S12. (a) Powder XRD patterns of As_2Se_3 deposited from solution and subsequently annealed to 350 °C, stick patterns correspond to orthorhombic As_2Se_3 (PDF no. 27-0027) and As_2Se_3 (PDF no. 26-0123); (b) Nyquist plot of As_2Se_3 film; Transient photoresponse of recovered (c) and pristine (d) As_2Se_3 film with chopped 1-Sun simulated illumination in contact with 0.1 M $Eu(NO_3)_3$ (aq).

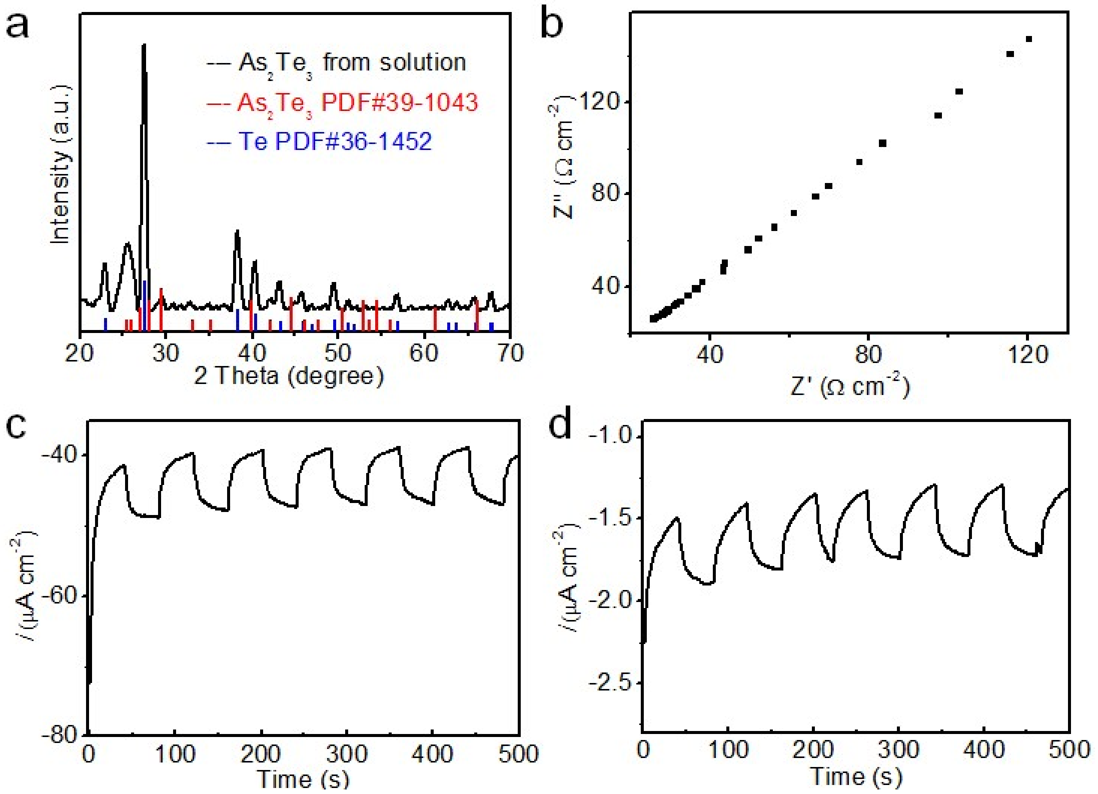

Figure S13. (a) Powder XRD patterns of As_2Te_3 deposited from solution and subsequently annealed to 350 °C, stick patterns correspond to orthorhombic As_2Te_3 (PDF no. 39-104303-065-2433) and Te (PDF no. 36-1452); (b) Nyquist plot of As_2Te_3 film; Transient photoresponse of recovered (c) and pristine (d) As_2Te_3 with chopped 1-Sun simulated illumination in contact with 0.1 M $Eu(NO_3)_3$ (aq).

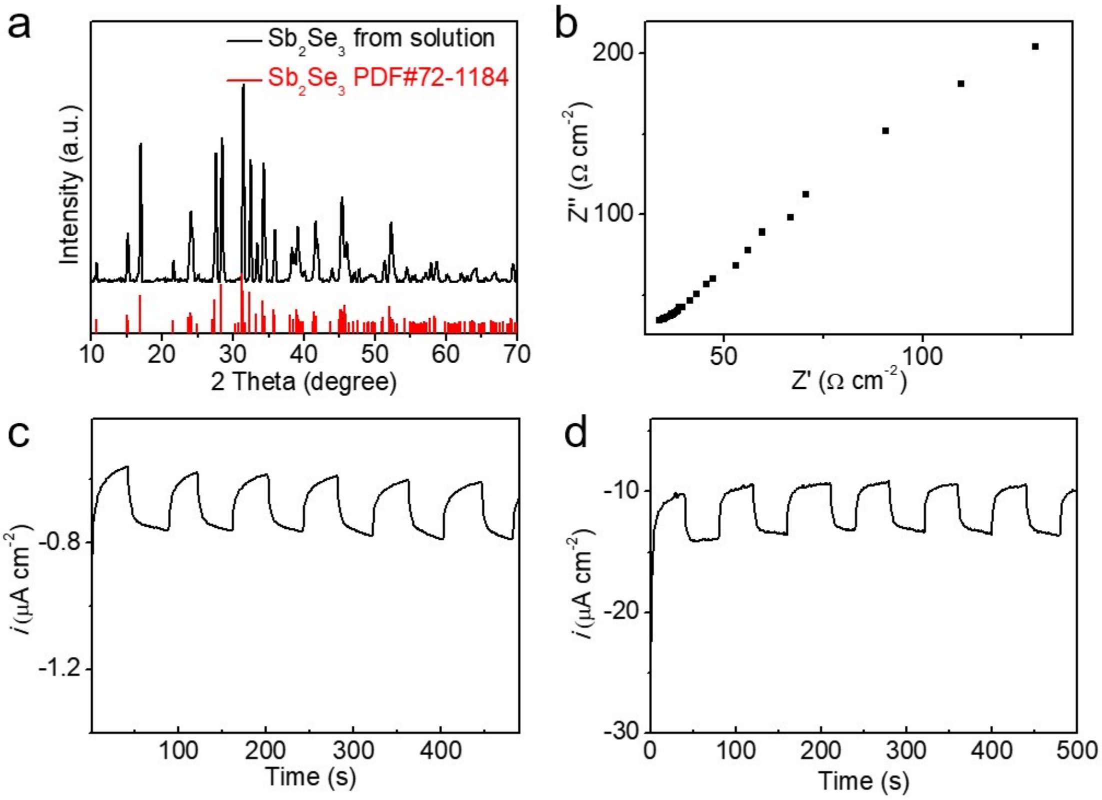

Figure S14. (a) Powder XRD patterns of Sb_2Se_3 deposited from solution and subsequently annealed to 350 °C and stick patterns correspond to orthorhombic Sb_2Se_3 (PDF no. 72-1184); (b) Nyquist plot of Sb_2Se_3 film; Transient photoresponse of recovered (c) and pristine (d) Sb_2Se_3 with chopped 1-Sun simulated illumination in contact with 0.1 M $Eu(NO_3)_3$ (aq).

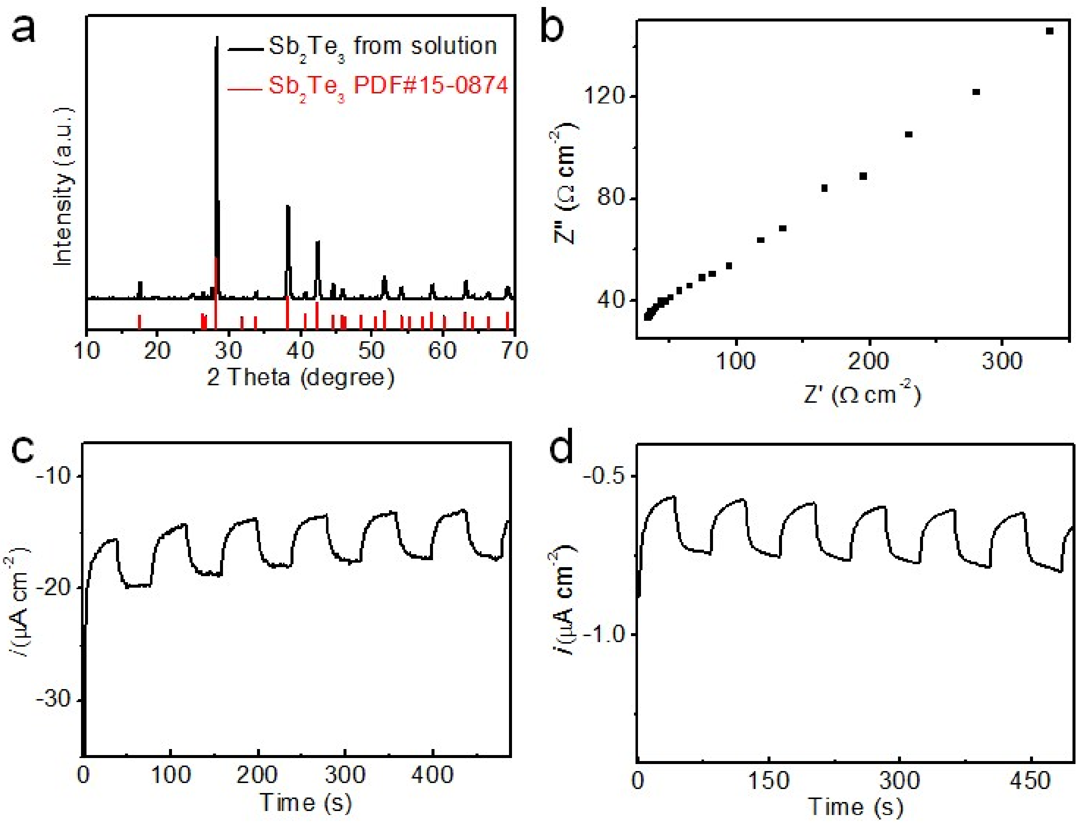

Figure S15. (a) Powder XRD patterns of Sb_2Te_3 deposited from solution and subsequently annealed to 350 °C and stick patterns correspond to orthorhombic Sb_2Te_3 (PDF no. 15-0874); (b) Nyquist plot of Sb_2Te_3 film; Transient photoresponse of recovered (c) and pristine (d) Sb_2Te_3 with chopped 1-Sun simulated illumination in contact with 0.1 M $Eu(NO_3)_3$ (aq).

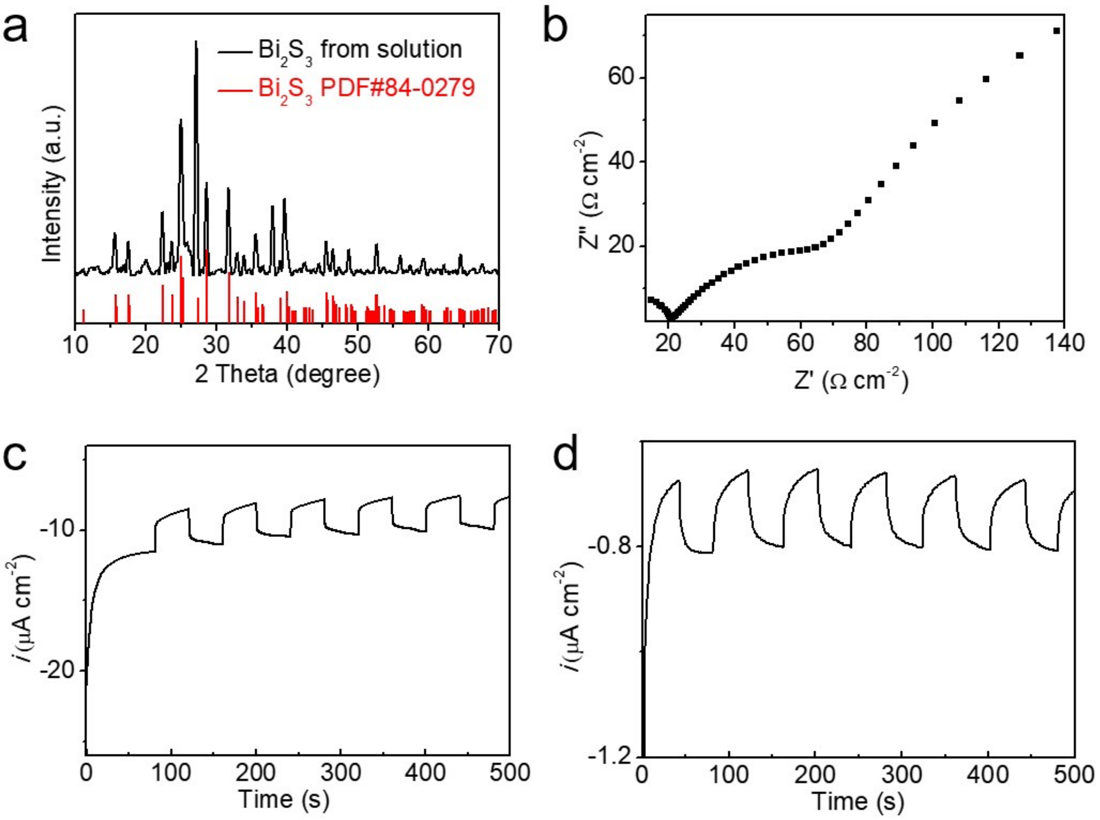

Figure S16. (a) Powder XRD patterns of Bi_2S_3 deposited from solution and subsequently annealed to 350 °C and stick patterns correspond to orthorhombic Bi_2S_3 (PDF no. 84-0279); (b) Nyquist plot of Bi_2S_3 film; Transient photoresponse of recovered (c) and pristine (d) Bi_2S_3 with chopped 1-Sun simulated illumination in contact with 0.1 M $Eu(NO_3)_3$ (aq).

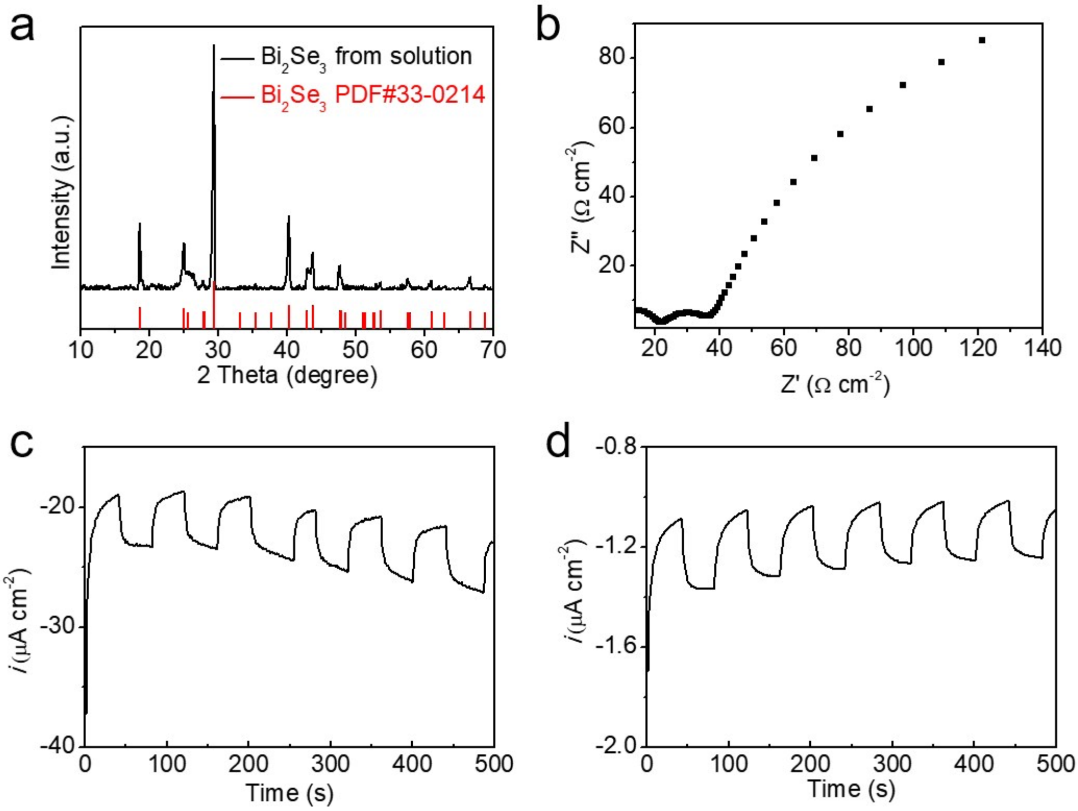

Figure S17. (a) Powder XRD patterns of Bi_2Se_3 deposited from solution and subsequently annealed to 350 °C and stick patterns correspond to orthorhombic Bi_2Se_3 (PDF no. 33-0214); (b) Nyquist plot of Bi_2Se_3 film; Transient photoresponse of recovered (c) and pristine (d) Bi_2Se_3 with chopped 1-Sun simulated illumination in contact with 0.1 M $Eu(NO_3)_3$ (aq).

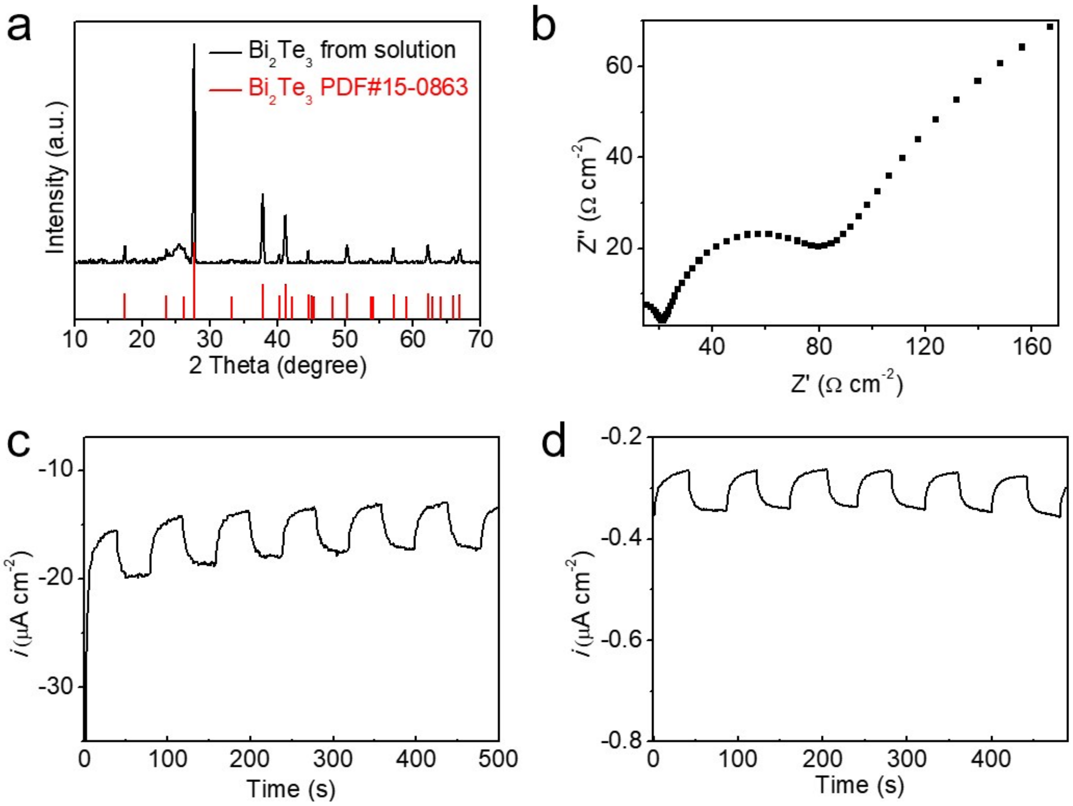

Figure S18. (a) Powder XRD patterns of Bi_2Te_3 deposited from solution and subsequently annealed to 350 °C and stick patterns correspond to orthorhombic Bi_2Te_3 (PDF no. 15-0863); (b) Nyquist plot of Bi_2Te_3 film; Transient photoresponse of recovered (c) and pristine (d) Bi_2Te_3 with chopped 1-Sun simulated illumination in contact with 0.1 M $Eu(NO_3)_3$ (aq).

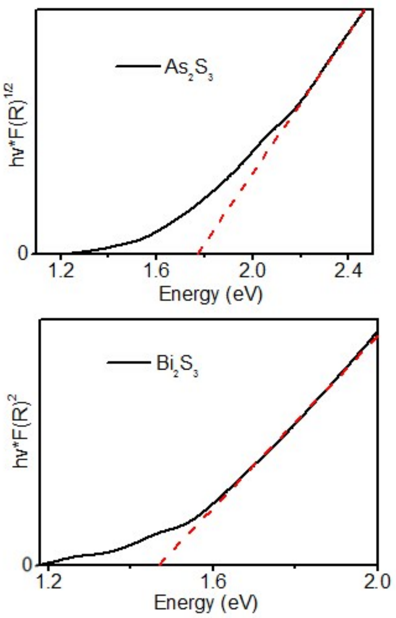

Figure S19. Tauc plot of the UV-vis-NIR transmission spectrum of spin-coated As_2S_3 and Bi_2S_3 films.

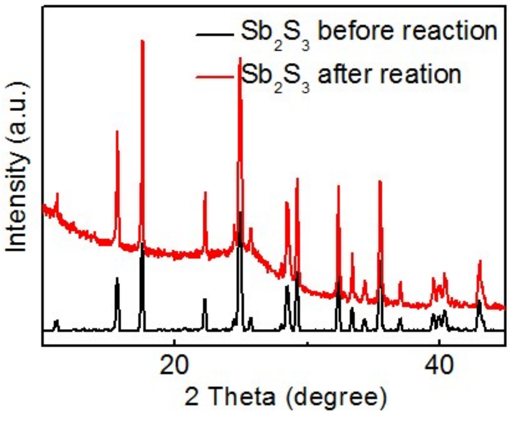

Figure S20. XRD patterns of Sb_2S_3 before and after reaction.

3. Supplementary Tables

Table S1. Solubility of all nine chalcogenides in the DBU/MTU solvent mixture

No.	t / day	T / °C	Solubility g/100 g solvent
As_2S_3	1	70	>3.5
As_2Se_3	2.4	70	1.83
As_2Te_3	3	85	0.8
Sb_2S_3	1.5	70	>2.6
Sb_2Se_3	2	70	>5
Sb_2Te_3	2	85	ca.1
Bi_2S_3	6	95	0.5
Bi_2Se_3	5	95	0.1
Bi_2Te_3	6	95	0.15

Table S2. Electron density (ρ_{BCP}), Laplacian of electron density ($\nabla^2\rho_{BCP}$), energy density (H_{BCP}) and eigenvalues (λ_1, λ_2 and λ_3) of Hessian matrix at corresponding bond critical point (ρ_{BCP}, $\nabla^2\rho_{BCP}$ and H_{BCP}, in a.u.).

Conform.	BCP	ρ_{BCP}	$\nabla^2\rho_{BCP}$	H_{BCP}	λ_1	λ_2	λ_3
DES	a1	0.0194	0.0536	-0.0002	0.0964	-0.0225	-0.0204
	a2	0.0241	0.0641	-0.0008	0.1218	-0.0299	-0.0278
DES-As_2S_3	b1	0.0549	0.0476	-0.0101	-0.0474	0.1400	-0.0449
DES-Bi_2Te_3	c1	0.0409	0.0634	-0.0048	0.1208	-0.0298	-0.0276
DES-Sb_2Se_3	d1	0.0479	0.0533	-0.0085	0.1233	-0.0362	-0.0339

Table S3. Kinetic parameters of transient absorption decays of Sb_2S_3 under 360 nm excitation with time profiles of absorption probed at 505 nm.

Decays	τ 1 (ps)	τ 2 (ps)	Average lifetime (ps)
Pristine Sb_2S_3	370 (91 %)	2300 (8 %)	525
Recovered Sb_2S_3	70 (77 %)	1050 (22 %)	290

4. References

1 Webber, D. H.; Brutchey, R. L. Alkahest for V_2VI_3 chalcogenides: dissolution of nine bulk semiconductors in a diamine-dithiol solvent mixture. *J. Am. Chem. Soc.* **2013**, *135*, 15722-15725.

2 Frisch, M.; Trucks, G.; Schlegel, H. B.; Scuseria, G.; Robb, M.; Cheeseman, J.; Scalmani, G.; Barone, V.; Mennucci, B.; Petersson, G., Nakatsuji H., Caricato M., Li X., Hratchian H. P., Izmaylov A. F., Bloino J., Zheng G., Sonnenberg J. L., Hada M., Ehara M., Toyota K., Fukuda R., Hasegawa J., Ishida M., Nakajima T., Honda Y., Kitao O., Nakai H., Vreven T., Montgomery J. J. A., Peralta J. E., Ogliaro F., Bearpark M., Heyd J. J., Brothers E., Kudin K. N., Staroverov V. N., Keith T., Kobayashi R., Normand J., Raghavachari K., Rendell A., Burant J. C., Iyengar S. S., Tomasi J., Cossi M., Rega N., Millam J. M., Klene M., Knox J. E., Cross J. B., Bakken V., Adamo C., Jaramillo J., Gomperts R., Stratmann R. E., Yazyev O., Austin A. J., Cammi R., Pomelli C., Ochterski J. W., Martin R. L., Morokuma K., Zakrzewski V. G., Voth G. A., Salvador P., Dannenberg J. J., Dapprich S., Daniels A. D., Farkas O., Foresman J. B., Ortiz J. V., Cioslowski J. and Fox D. J. Gaussian 09, Revision A. 02, Gaussian. *Inc., Wallingford, CT* **2009**, *200*.

3 Krishnan, R.; Binkley, J. S.; Seeger, R.; Pople, J. A. Self-consistent molecular orbital methods. XX. A basis set for correlated wave functions. *J. Chem. Phys.* **1980**, *72*, 650-654.

4 Wadt, W. R.; Hay, P. J. Ab initio effective core potentials for molecular calculations. Potentials for main group elements Na to Bi. *J. Chem. Phys.* **1985**, *82*, 284-298.

5 FU, R.; LU, T.; CHEN, F.-W. Comparing methods for predicting the reactive site of electrophilic substitution. *Acta. Phys.-Chim. Sin.* **2014**, *30*, 628-639.

6 Cao, B.; Du, J.; Liu, S.; Zhu, X.; Sun, X.; Sun, H.; Fu, H. Carbon dioxide capture by amino-functionalized ionic liquids: DFT based theoretical analysis substantiated by FT-IR investigation. *RSC Adv.* **2016**, *6*, 10462-10470.

7 Bader, R. F. Atoms in molecules. *Accounts. Chem. Res.* **1985**, *18*, 9-15.

8 Cao, B.; Du, J.; Cao, Z.; Sun, X.; Sun, H.; Fu, H. DFT study on the dissolution mechanisms of α-cyclodextrin and chitobiose in ionic liquid. *Carbohyd. Polym.* **2017**, *169*, 227-235.

9 Lu, T.; Chen, F. Multiwfn: a multifunctional wavefunction analyzer. *J. Comput. Chem.* **2012**, *33*, 580-592.

10 Jessop, P. G.; Jessop, D. A.; Fu, D. B.; Phan, L. Solvatochromic parameters for solvents of interest in green chemistry. *Green. Chem.* **2012**, *14*, 1245-1259.

11 Lungwitz, R.; Spange, S. A hydrogen bond accepting (HBA) scale for anions, including room temperature ionic liquids. *New. J. Chem.* **2008**, *32*, 392-394.

12 Hauru, L. K.; Hummel, M.; King, A. W.; Kilpelainen, I.; Sixta, H. Role of solvent parameters in the regeneration of cellulose from ionic liquid solutions. *Biomacromolecules* **2012**, *13*, 2896-2905.

13 Reichardt, C. Solvatochromic Dyes as Solvent Polarity Indicators. *Chem. Rev.* **1994**, *94*, 2319-2358.

14 Kolling, O. W. Spectrophotometric measurement of solvent polarity with phenol blue as the probe. *Anal. Chem.* **1981**, *53*, 54-56.

15 Xue, Z. H.; Han, J. T.; Feng, W. J.; Yu, Q. Y.; Li, X. H.; Antonietti, M.; Chen, J. S. Tuning the Adsorption Energy of Methanol Molecules Along Ni-N-Doped Carbon Phase Boundaries by the Mott-Schottky Effect for Gas-Phase Methanol Dehydrogenation. *Angew. Chem. Int. Ed.* **2018**, *130*, 2727-2731.

16 Ghosh, C.; Varma, B. Optical properties of amorphous and crystalline Sb_2S_3 thin films. *Thin solid films* **1979**, *60*, 61-65.

17 Wang, B.; Qin, L.; Mu, T.; Xue, Z.; Gao, G. Are Ionic Liquids Chemically Stable? *Chem. Rev.* **2017**,

117, 7113-7131.

18 Abbott, A. P.; Capper, G.; Davies, D. L.; Rasheed, R. K.; Tambyrajah, V. Novel solvent properties of choline chloride/urea mixtures. *Chem. Comm.* **2003**, 70-71.

19 Fotakis, G.; Timbrell, J. A. In vitro cytotoxicity assays: comparison of LDH, neutral red, MTT and protein assay in hepatoma cell lines following exposure to cadmium chloride. *Toxicol. Lett.* **2006**, *160*, 171-177.

20 Tafazoli, S.; Mashregi, M.; O'Brien, P. J. Role of hydrazine in isoniazid-induced hepatotoxicity in a hepatocyte inflammation model. *Toxicol. Appl. Pharm.* **2008**, *229*, 94-101.

21 J. Wang, P. Wang, Q. Wang, H. Mou, B. Cao, D. Yu, D. Wang, S. Zhang and T. Mu, *ACS Sustain. Chem. Emg.*, 2018.